Numerical Simulation of Cross-Flow in Tube-Bundles to Model Flow Circulation of the Moderator in CANDU-6

R. Necciari[1], A. Teyssedou[1] and M. Reggio[2]
[1] Nuclear Engineering Institute, Engineering Physics Department,
École Polytechnique de Montréal, Montréal, Québec, Canada
[2] Mechanical Engineering Department,
École Polytechnique de Montréal, Montréal, Québec, Canada

Abstract

The knowledge of external wall temperature distributions around calandria tubes is a major concern during normal and off-normal operating conditions of CANDU power reactors. To this aim, the use of Computational Fluid Dynamics (CFD) techniques to model moderator local flow velocities and temperatures can largely help in performing nuclear safety analyses. However, present numerical codes applied for this purpose makes use of the well known porous media approach. This method necessitates a previous knowledge of distributed hydraulic resistances that must be obtained from appropriate scaled experiments. Within this framework, this paper presents a set of 2D CFD simulations of incompressible cross-flows along in-line and staggered tube bundles. The numerical results are validated against experimental data obtained from the open literature. Calculations are performed using FLUENT-6 code. The Reynolds-Average Navier Stokes (RANS) equations are used in conjunction with several turbulence models and both the SIMPLE (Semi-Implicit Pressure Linked Equation) as well as the coupled pressure-based algorithm. In general, it is observed that two-equation turbulence models are able to reproduce mean velocities. Even though reasonably good predictions of flow distributions along staggered tube set-ups are obtained, the predictions of the pressure drop along in-line tubes are in general not satisfactory. In most cases, the coupled pressure-based algorithm seems to perform better but requires longer computation time. In general, the standard κ-ε is superior to others κ-ε models. The κ-ω model behaves better for fairly well developed flows.

1. Introduction

The knowledge of flow velocity and temperature distributions of the moderator in the vessel of CANDU-6 reactors is important in nuclear safety analysis. The correct simulation of local fluid velocities around calandria tubes should permit heat transfer conditions to be predicted. However, the multi-connected structure of the calandria region makes numerical simulations to be difficult and costly. In order to deal with this problem, a porous media approach that replaces calandria tubes by appropriate hydraulic resistances was introduced in the 1980's. Thus, the Canadian nuclear industry developed the MODTURC (MODerator TURbulent Circulation [1]) and MODTURC-CLAS (MODerator TURbulent Circulation Co-Located Advanced Solution [2]) codes. MODTURC_CLAS was validated by Yoon et al. [3-5] using pressure loss data collected for incompressible flows along in-line and staggered tube-bundles. The experiments [6] used a quarter scale test section to simulate an axial slice of a CANDU vessel. The in-line bundle is composed of 24 rows while the staggered one contains 33 rows. Porous model calculations only

provide average values of flow velocities and temperatures. In fact these methods do not give information of local flow variables near solid walls, necessary to implement heat transfer calculations. The FLUENT code was used to model moderator's flow across all calandria tubes [7], however, it has been pointed out that the calculations are extremely sensitive to inlet water-jet conditions [8]. The huge difference in dimensions that exists between the geometry of the nozzles (i.e., few centimeters) and the calandria itself (i.e., several meters) makes the entire simulations almost impossible to be properly performed. Further, the representation of turbulent jet dynamics requires a mesh structure quite different to that used for calandria tubes. Bouquillon proposed a semi-analytical nozzle model to be implementing in future CFD simulations of moderator's flow. This approach should permit an appropriate mesh of the multi-connected region to be used, without the necessity of numerically modeling nozzle flows. Due to the geometrical arrangement of calandria tubes, almost cross-flow distributions will develop around calandria tubes. Cross-flow visualizations have been investigated among others by Zukauskas [9] who has also proposed pressure drop and heat transfer correlations. A detailed review of this kind of flows can be found in references [10, 11-14]. Most flow visualizations are performed in tube bundles having little number of rows. From a numerical simulation viewpoint, several studies were carried out [15, 16]; a detailed review is given in references [11-14]. The present work is two-folds: first to validate 2D cross-flow simulations with data collected in both in-line and staggered tube-bundles, and second to optimize different numerical schemes to treat Hadaller et al. [6] experiments. To fulfill these goals, the validation is performed by using flow velocity data given in references [11-13]. For the pressure drop, data given in [15] are selected. Simulations are carried out using FLUENT-6 with the following steady-state turbulence models: *i*) κ-ε, *ii*) κ-ε realizable, *iii*) κ-ε RNG and *iv*) κ-ω.

2. Description of selected experimental data

Experimental data given in references [6, 11-13, 15] are simulated; the experimental set-ups are schematically shown in Figure 1, and key parameters are summarized in Table 1.

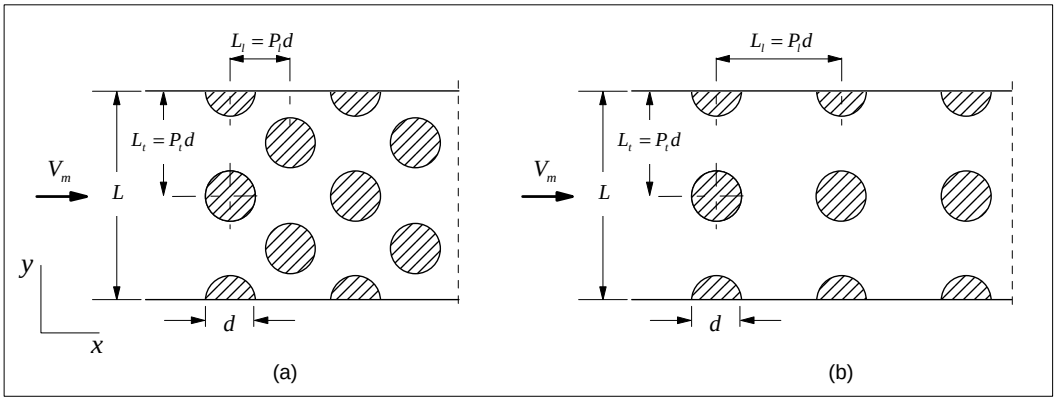

Figure 1. Schematics of: (a) staggered and (b) in-line tube-bundles.

In all cases, the test sections have rectangular or square geometry. The experiments selected for the present study are performed using water under constant temperature conditions and uniform inlet velocity with Reynolds number based on cylinder diameter and this velocity. Paul et al. [11-13] used a PIV (Particle Image Velocimetry) technique while Balabani & Yianneskis [15] used

LDA (Laser Doppler Anemometry) to collect local velocity data. None of them provide information on neither the pressure measurement technique they have used nor the locations of the pressure taps. Thus, to compare the simulations with pressure data, this information is obtained from correlations proposed by the authors.

The present numerical study considers only 2D flow simulations; thus, it is expected that the results could not fully reproduce the experimental trends. In this paper, data of configurations 1 and 2 of Balabani & Yianneskis [15] and three flow configurations of Hadaller et al. [6] are used to perform the validation.

Table 1. Summary of key experimental parameters.

	Balabani & Yianneskis [15] Config. 1	Balabani & Yianneskis [15] Config. 2	Balabani & Yianneskis [15] Config. 3	Paul et al. [11-13]	Hadaller et al. [6] Config. 1		Hadaller et al. [6] Config. 2
Type*	I	S	S	S	S		I
Number of rows	5	6	6	6	33		24
Number of arrays	3	3 ; 2	3 ; 2	3 ; 2	4 ; 3		4
L (mm)	72	72	72	193.04	346		286
Depth (mm)	72	72	72	200	200		200
d (mm)	10	10	10	25.4	33.02		33.02
L_l (mm)	36	36	36	53.34	50.49		71.4
L_t (mm)	21	21	16	96.52	100.98		71.4
P_l	3.6	3.6	3.6	2.1	≈1.53		≈2.16
P_t	2.1	2.1	1.6	3.8	≈3.06		≈2.16
$V_m(m/s)$	0.930	0.930	0.930	0.340	0.054	0.070	0.103
$T(^oC)$	20.0	20.0	20.0	23.0	39.5	63.6	79.8
Re	9255	9255	9255	9300	2746	5237	9392

* I = in-line, S = staggered

3. Modelling equations

The governing equations used in FLUENT are based on the RANS equations (Reynolds Average Navier-Stokes). For 2D steady state incompressible flows the conservation equations for mass and momentum are written as:

$$\frac{\partial U_i}{\partial x_i} = 0 \tag{1}$$

$$\rho \frac{\partial (U_i U_j)}{\partial x_i} = -\frac{\partial P}{\partial x_j} + \frac{\partial}{\partial x_i}(\mu \frac{\partial U_j}{\partial x_i} - \rho \overline{u_i u_j}) + \rho \overline{f_j} \tag{2}$$

where $\overline{f_j}$ represents average values of body forces, U_i is the average i velocity component, P is the mean pressure and $\overline{u_i u_j}$ is the ij component of the Reynolds stress tensor. It must be pointed out that for the purpose of the present study body forces are equal to zero. In addition, turbulence

models are based on Boussinesq's hypothesis that links the Reynolds stress tensor to a turbulent viscosity (or eddy-viscosity); thus:

$$\overline{u_i u_j} = \nu_t \left(\frac{\partial U_j}{\partial x_i} + \frac{\partial U_i}{\partial x_j} \right) - \frac{2}{3} \delta_{ij} \kappa \tag{3}$$

where ν_t is the turbulent viscosity which is not constant, κ is the turbulent kinetic energy and δ_{ij} is the Kronecker delta function. Equations (1-3) represent a system of three equations with five unknowns; thus, its solution requires two additional closure relationships. It is a common practice to model these relations under the form of transport equations for turbulence production (i.e., κ) and dissipation. (i.e., ε or ω). Their solution, however, is not possible without introducing new parameters that are in general determined experimentally. The choice of these relations permits different turbulent models to be applied. In the present study the following turbulence models are used: *i*) the standard κ-ε model proposed by Launder & Spalding [17], *ii*) the κ-ε realizable introduced by Shih et al. [18], *iii*) the κ-ε RNG introduced by Yakhot & Orszag [19] and *iv*) the standard κ-ω based on the work of Wilcox [20]. It must be pointed out that the Shear-Stress Transport κ-ω model proposed by Menter [21] was also used; however, in all the cases its convergence rate was difficult to achieve and it was not able to produce satisfactory results (these results are not discussed in this paper). Finally, to close the system of equations, the eddy-viscosity ν_t is calculated using other constitutive relations that necessitate previous values of κ and ε or/and ω. For more information, interested readers can consult FLUENT's User Guide [22]. FLUENT uses a finite volume approach to solve conservation equations and it offers to the user several discretization schemes. In these schemes pressures are estimated by interpolating the values obtained from momentum conservation equations. The following interpolation techniques are available: standard, second-order, body-force-weighted and PRESTO! (PREssure STaggering Option). The standard method applies a linear interpolation, the second-order technique uses a cell-centered difference while in the body-force-weighted approach normalized pressure gradients and body forces are assumed to be constant. These schemes use non staggered control volumes, instead, PRESTO! is based on staggered domains where pressures are computed over the faces of the volumes. Previous numerical tests have shown that in general, PRESTO! and body-force-weighted schemes provide better results than the standard and the second-order ones; thus, PRESTO! is used in the rest of this work. Five schemes are also offered to the user for solving convection terms: a first-order upwind power-law, a second-order upwind discretization, as well as third order methods QUICK and MUSCL (Monotone Upstream-Centered Schemes for Conservation Laws). We have observed that second-order schemes are equivalent to the third-order and perform much better than first-order ones. For this reason, a second-order upwind scheme is selected to perform simulations. Further, pressure-based and density-based solvers are available in FLUENT. Since the present study concerns incompressible flows, the pressure-based solver is used. In addition, the following segregated type algorithms: SIMPLE, SIMPLEC, PISO and FSM as well as a coupled one are proposed in the FLUENT user's manual. The SIMPLE algorithm developed by Patankar [23], establishes a relationship between the flow velocity field and pressure corrections to ensure overall mass balance conditions. Further, the simulations performed using SIMPLE are compared with those obtained with the Coupled pressure-based algorithm.

For all cases studied, the residuals are considered as a convenient convergence metrics. Hence, calculations are considered to converge when residuals show a decreasing trend or they stay constant around 10^{-5}. In addition, for key physical variables such as the flow velocities and pressures their relative variations must be lower than 10^{-3} *m/s* and 1 *Pa* respectively, before stopping the calculations.

4. Computational meshes

The domain of integration is discretized using GAMBIT, which is the companion preprocessor of FLUENT. Similar to the work of Paul et al. [11-13], virtual lengths are added both at the inlet and at the outlet of the experimental set-ups. The first allows a velocity profile to be fully developed at the entrance of the tube-bundle region while the second ensures complete turbulence dissipation to occur in the outlet zone. To simulate Paul et al. and Balabani & Yianneskis [15] experiments, extended lengths (relative to the first or the last row of tubes) equivalent to ten cylinder diameter are used. Instead for the staggered case of Hadaller et al. [6], a much longer length is applied, especially to handle the κ-ω turbulence model. (=27.5 *d*). Uniform inlet flow velocity is used as boundary condition. No-slip conditions are used over solid walls and an outflow condition is applied at the outlet of the channel. Turbulence is modeled based on the hydraulic diameter equals to the inlet channel diameter, with a turbulent intensity of 4%. Furthermore, for turbulence models, an enhanced wall treatment is used to allow viscosity changes near-wall regions to be taken into account [23]. The laminar sub-layer is treated as a non-dimensional distance to the first wall-adjacent cell, defined by:

$$y^+ = \frac{\rho u_\tau y_P}{\mu} \tag{4}$$

where y_P is the distance from cell *P* to the solid wall, μ is the dynamic viscosity and u_τ is the friction velocity that is calculated as:

$$u_\tau = \sqrt{\frac{\tau_w}{\rho}} \tag{5}$$

with τ_w the wall-shear stress. Within the laminar sub-layer y^+ should be close to 1 and lower than 5. Because the particular geometry of the experimental set-ups, it is difficult to satisfy this condition over the channel walls (i.e., regions without cylinders) where y^+ can reach values of up to 12. Nevertheless, the overall flow is mostly conditioned by the presence of cylinders than the walls of the channel. For instance, Hadaller et al. [6] noticed that frictional pressure losses due to channel walls are negligible, as compared to those caused by the cylinders themselves. This is confirmed by previous numerical experiments we have performed using different mesh refinements (e.g., $5 < y^+ < 12$) around the walls, where no noticeable differences were obtained. It must be pointed out that for cylinder walls y^+ is always within the right range (i.e., close to 1).

5. Study the effect of mesh structures and densities

Several mesh constructions obtained by a geometrical decomposition of the integration domain, are studied. Most of the simulations are performed by using mesh elements similar to those

shown in Figure 2. Around the cylinders, these are multi-block quadrilateral structured meshes obtained by placing a cylinder inside a square (Fig. 2a). This arrangement makes it possible to refine the mesh close to cylinder walls by controlling the mesh vertex position on virtual edges placed on the diagonal lines. Several problems are associated to this type of discretization. The numbers of cells considerably increases with increasing the refinement near the walls of the duct. Due to the difference of transverse and longitudinal pitch ratios, an apparent mesh discontinuity on the corners of the squares surrounding the cylinders is produced. Finally, meshes generated between the points belonging to diagonal lines, do not follow the curvature of the cylinders. It is obvious that this drawback provokes the formation of some kind of concentration poles near cylinders, between each two consecutive diagonals. To overcome these difficulties an enhancement of the mesh shown in Figure 2b is introduced. This new cell structure makes it possible to avoid discontinuities on the corner of the squares surrounding the cylinders and to provide better values of $y+$ over channel walls. Numerical tests are then performed by using both structures of Figure 2. The comparisons between the results obtained with these two schemes and κ-ε and κ-ω turbulence models, indicate that the differences are not significant. Therefore, the enhanced mesh structure shown in Figure 2b is adapted. To determine the effect of the geometry of the cells on the simulations, a series of numerical tests are performed. It is important to mention, that for comparison purposes in these tests the structure shown in Figure 2a is also used. During a first step the effect of mesh refinement is studied (Table 2); thereafter, similar simulations are carried out using other mesh geometries summarized in Table 3. Experimental conditions given in Paul et al. [11-13] (Table 1) in conjunction with the SIMPLE algorithm are used to perform this part of the simulations. Herewith, mesh 2 that corresponds to the structure shown in Figure 2a is considered as a reference case. In turn, mesh 3 refines the domain mainly in the vicinity of the cylinders whereas mesh 4 is able to refine also regions close to duct walls. It is apparent that the first mesh is coarser than the others.

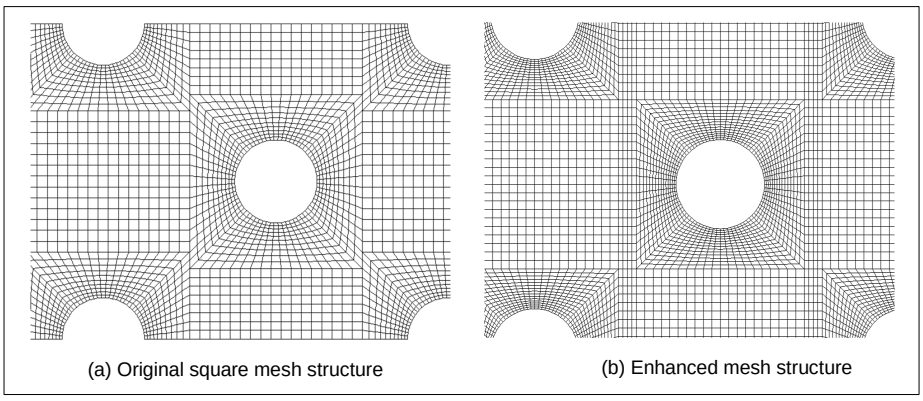

Figure 2. Square-based discretization cells.

Non-dimensional average streamwise velocity profiles are computed along the following surfaces: *i*) wake zone of rows 1 and 3, *ii*) impact zone of rows 3 and 5, *iii*) at normalized distance x/d=1.25 and *iv*) normalized distance x/d= 7.55. Similarly, non-dimensional average transverse velocity profiles are computed at distances x/d=1.25 and x/d= 7.55 (Figure 3). Results obtained with the κ-ε RNG turbulence model are compared in Figure 4, while the simulations carried out using the κ-ω model are shown in Figure 5.

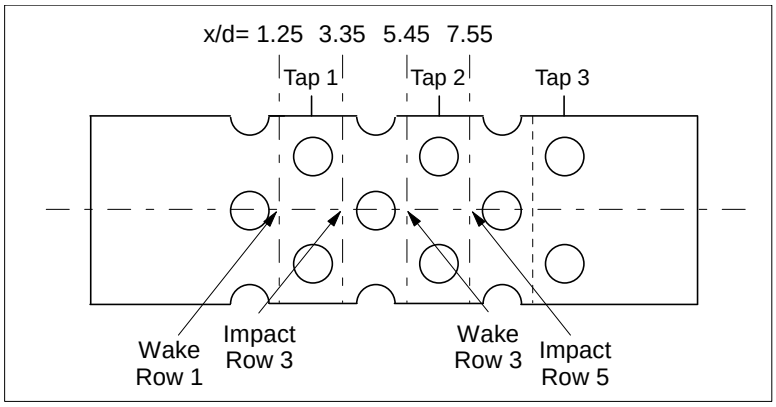

Figure 3. Paul et al. [13] flow channel and locations where the results of the simulations are sampled.

Table 2. Principal properties of different square-based mesh structures.

		Mesh 1	Mesh 2	Mesh 3	Mesh 4
Number of cells		113760	199440	290000	530400
Intervals around cylinders		240	320	400	560
Intervals on diagonals (first ratio)		40 (1.05)	60 (1.05)	70 (1.05)	100 (1.03)
Maximum area ($10^{-3}\,m^2$)		1.38	1.3	1.23	1.34
Minimum area ($10^{-5}\,m^2$)		11.5	3.95	2.37	2.3
Maximum Aspect Ratio (< %5)		3.47 (100)	6.34 (97.83)	8.42 (94.21)	6.3 (97.685)
Maximum y+ over channel wall (average values)	κ-ε Real.	14.82 (6.9)	12.5 (4.78)	10.85 (3.7)	8.8 (2.35)
	κ-ε RNG	14.8 (6.9)	12.49 (4.7)	10.84 (3.74)	8.8 (2.44)
	κ-ω	14.75 (8.32)	12.29 (5.69)	10.74 (4.35)	8.72 (2.4)
Maximum y+ over cylinders (average values)	κ-ε Real.	7.19 (2.7)	2.47 (0.92)	1.48 (0.55)	1.44 (0.53)
	κ-ε RNG	7.19 (2.7)	2.48 (0.93)	1.49 (0.56)	1.44 (0.54)
	κ-ω	7.49 (2.49)	5.69 (0.85)	1.58 (0.5)	1.54 (0.49)

The κ-ε RNG turbulence model in conjunction with meshes 2, 3 and 4 produces quite similar results. Some differences are observed in the velocity profiles in the wake zone of row 3 and the impact zone of row 5 when the coarsest mesh 1 is used. Similar trends, not shown in the figure, are also observed when the κ-ε Realizable model is applied. When the κ-ω model is implemented, Figure 5 shows that the differences among the results obtained with mesh 1 with respect to the other ones, are still present. It is apparent that mesh 1 is too coarse; it does not satisfy the maximum allowable value of y^+ around cylinders. Furthermore, it must be pointed out that the data of Paul et al. represent only half of the experimental set-up; thus, only half of the integration domain is discretized. However, additional numerical experiments not presented in this paper, indicate that the simulation of the entire domain produces not only different but much better results than using symmetric boundary conditions. This observation is more apparent when the κ-ω turbulence model is implemented. In general, with this turbulence model all meshes produce relatively different results except for the streamwise velocity at the x/d plane (Figures 5e to 5h); slight dissimilarities occur at x/d=7.55 when mesh 4 is used. Nevertheless, a detailed analysis of numerical results is not straightforward because the κ-ω model does not produce good

outcomes when half of the domain is treated. For this reason, in the remaining part of this study, entire flow channels are simulated.

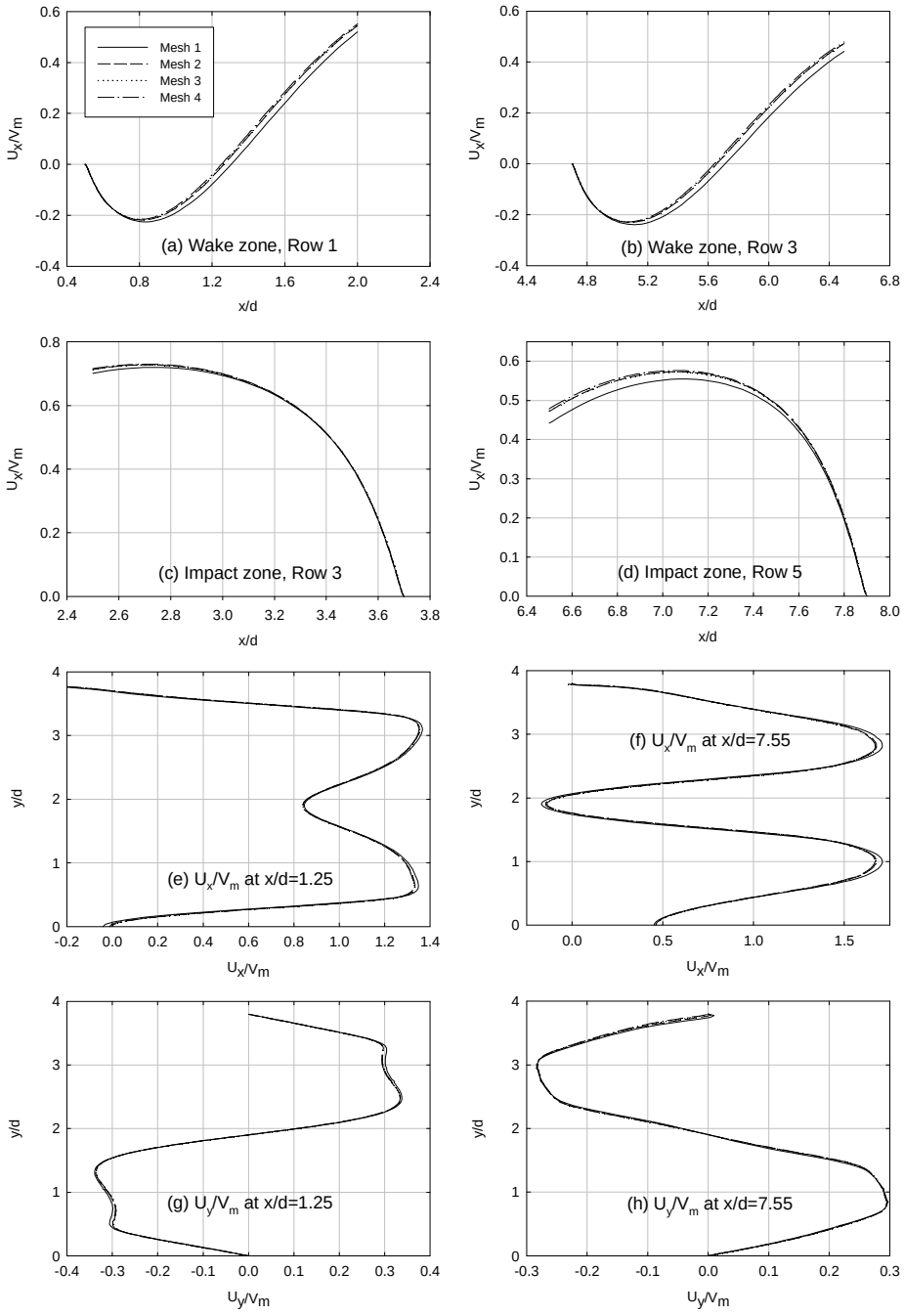

Figure 4. Numerical tests carried out using the κ-ε RNG turbulence model.

We have observed that the κ-ω model is more sensitive to the mesh structure than κ-ε one. Moreover, the enhanced mesh 2, shown in Figure 2b, in conjunction with the κ-ε turbulence

model, generates the best results and requires less calculation time. In turn, meshes 3 and 4 are more costly and they do not necessarily improve the predictions.

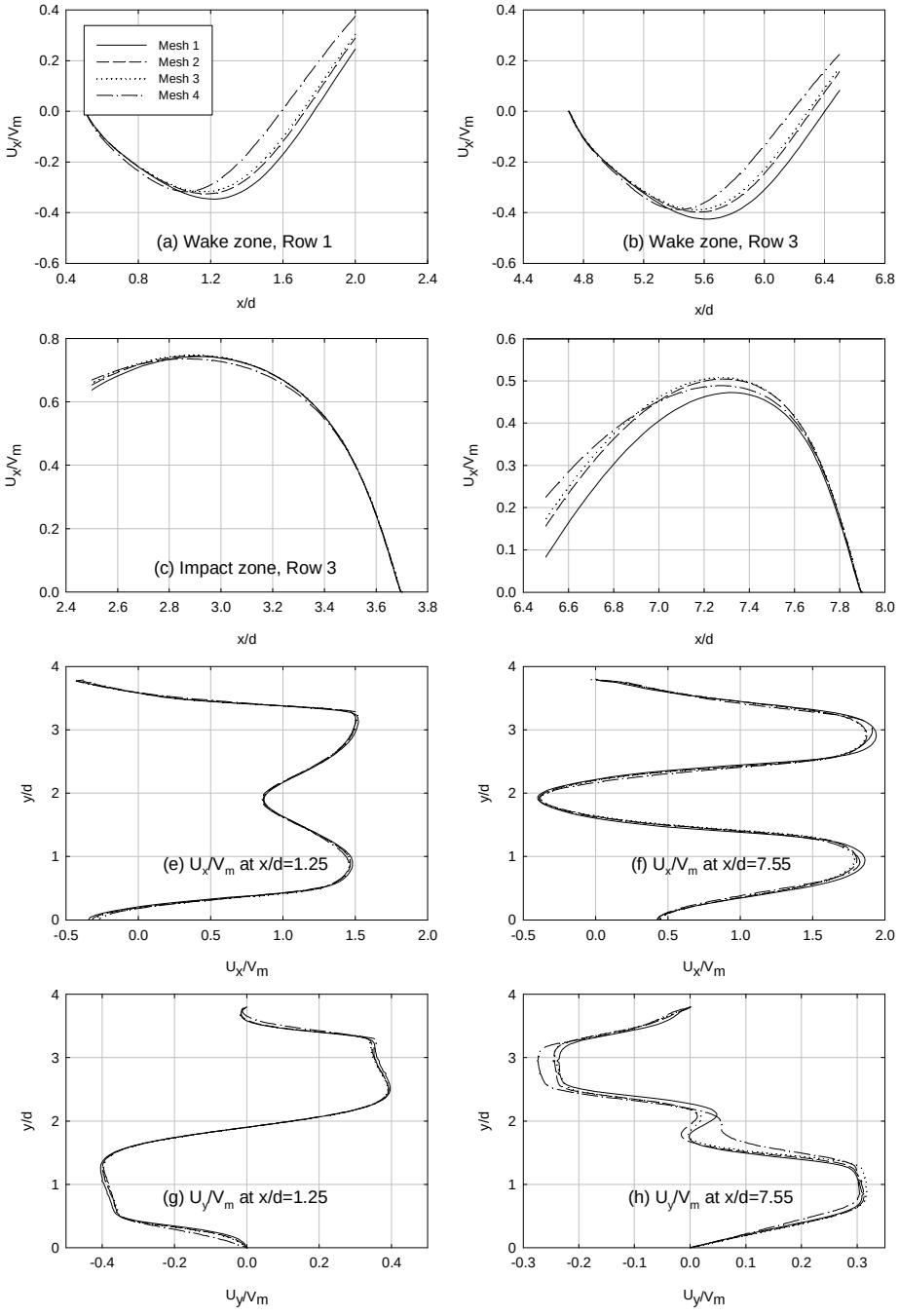

Figure 5. Numerical tests carried out using the κ- ω turbulence model.

In addition to the former numerical experiments, circular, hybrid and triangular cell geometries are also tested against flow conditions given in Paul et al. [11-13]. In particular circular cells, shown in Figure 6a, allow the pole concentration phenomena to be eliminated. The hybrid structure shown in Figure 6b is obtained by combining circular discretization with an additional

geometrical decomposition of the domain. Finally, the unstructured triangular mesh used in this work is given in Figure 6c. Note that the hybrid structure is coarser than the other ones. To satisfy required values of y^+, triangular meshes necessitate a large number of cells, which increases the calculation time. For a given turbulence model, it is observed that the convergence is more difficult to reach when hybrid and triangular structures are used. In order to reach convergence, the Coupled algorithm is implemented in FLUENT. Similar to the former numerical experiments, non-dimensional average streamwise velocity profiles are computed along the following surfaces: *i*) wake zone of Rows 1 and 3, *ii*) impact zone of rows 3 and 5, *iii*) at normalized distance x/d=1.25 and *iv*) normalized distance x/d= 7.55 (Figure 3). Non-dimensional average transverse velocity profiles are computed at distances x/d=1.25, x/d=3.35, x/d=5.45 and x/d=7.55. Results obtained with the κ-ε Realizable turbulence model are compared in Figures 7 and 8.

Table 3. Principal properties of additional mesh structures.

Mesh type		Enhanced (Square-based)	Circular	Hybrid	Triangular
Number of cells		771000	528000	340400	1 224896
Intervals over cylinders		400	320	240	800
Maximum area ($10^{-3}\ m^2$)		1.25	2.7	2.3	4
Minimum area ($10^{-5}\ m^2$)		2.25	2.3	7.9	3.87
Maximum aspect ratio (under 5%)		8 (96.82)	9.1 (89.795)	4.86 (100)	7.2 (99.76)
Maximum y+ over channel wall (average values)	κ-ε	4.27 (.91)	7.8 (2.6)	10.1 (4.2)	8.12 (1.42)
	κ-ε Real.	4.27 (.85)	7.8 (2.3)	10.1 (3.9)	8.12 (1.34)
	κ-ε RNG	4.27 (.85)	7.9 (2.4)	10.1 (4)	8.12 (1.34)
	κ-ω	4.27 (.88)	7.8 (2.6)	10.13 (4.6)	8.03 (1.34)
Maximum y+ over cylinders (average values)	κ-ε	1.68 (.65)	0.99 (0.52)	2.9 (1.5)	2.5 (1.23)
	κ-ε Real.	1.64 (.61)	0.97 (0.49)	2.89 (1.45)	2.43 (1.16)
	κ-ε RNG	1.64 (.62)	0.97 (.5)	2.85 (1.45)	2.44 (1.18)
	κ-ω	1.82 (.61)	1 (0.47)	3.16 (1.36)	2.76 (1.1)

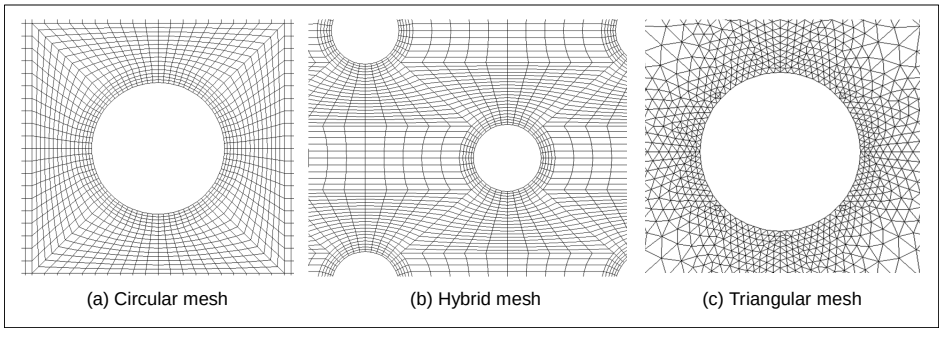

Figure 6. Mesh structures: (a) Circular; (b) Hybrid; (c) Triangular.

It can be seen that the four types of meshes generate almost the same results. In turn, simulations performed with the κ-ω model, shown in Figures 9 and 10, seem to be quite sensitive to the discretization of the integration domain. It must be pointed out that for this turbulence model, Paul et al. [11-13] have arrived to the same observation.

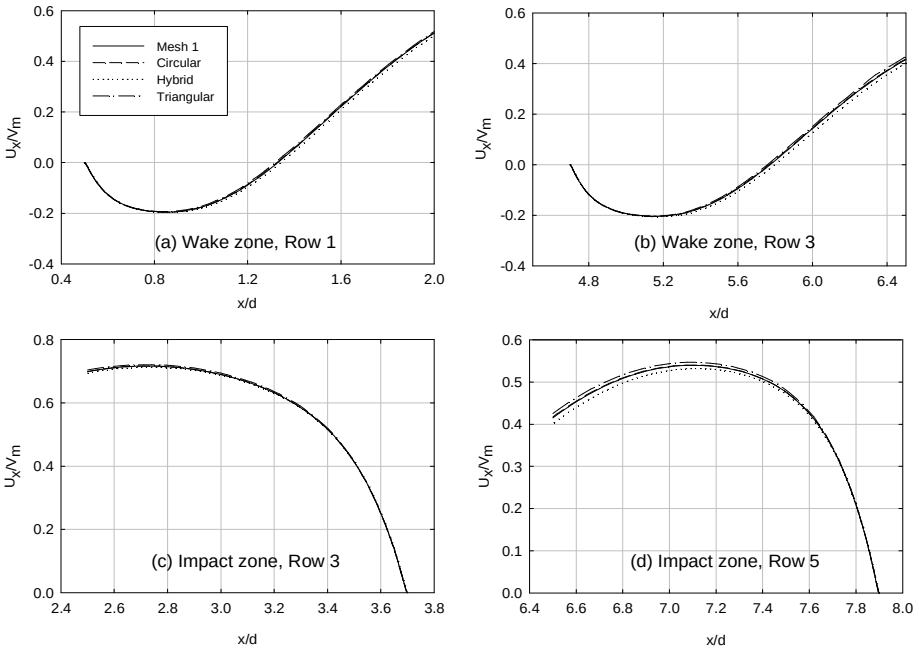

Figure 7. Simulations performed with the κ-ε Realizable turbulence model (non-dimension axial location with respect to row 1, y/d=0).

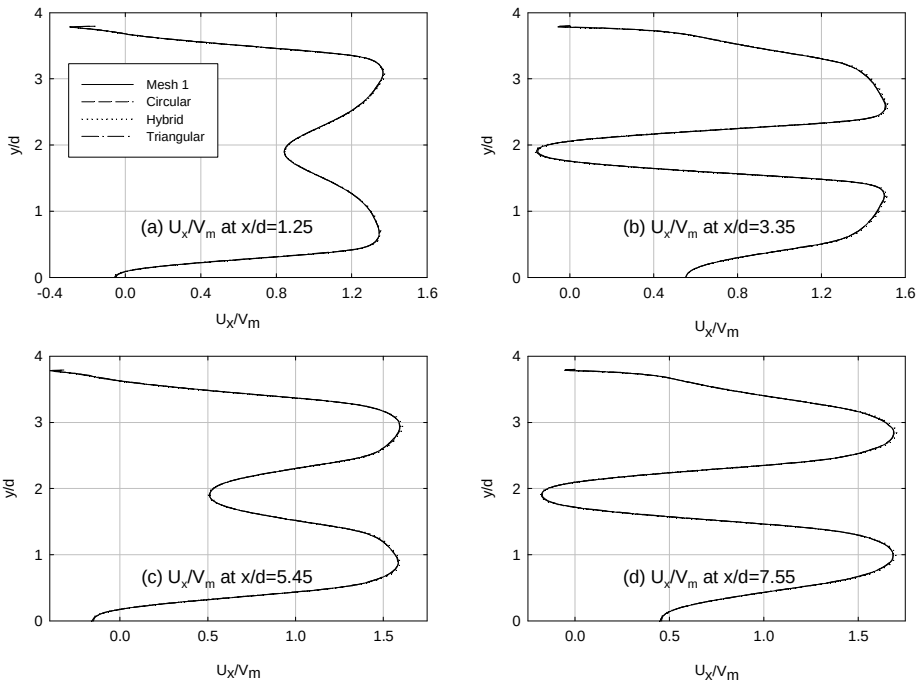

Figure 8. Simulated streamwise velocity profiles obtained with the κ-ε Realizable turbulence model (x/d = 1.25, 3.35, 5.45 and 7.55).

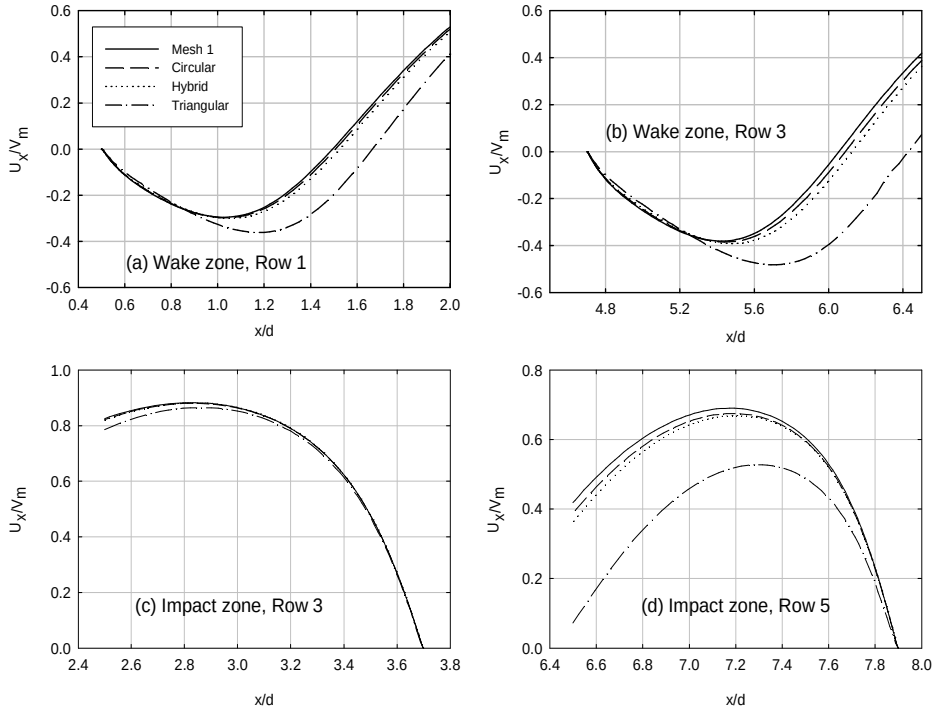

Figure 9. Simulations performed with the κ-ω turbulence model (non-dimension axial location with respect to row 1, y/d=0).

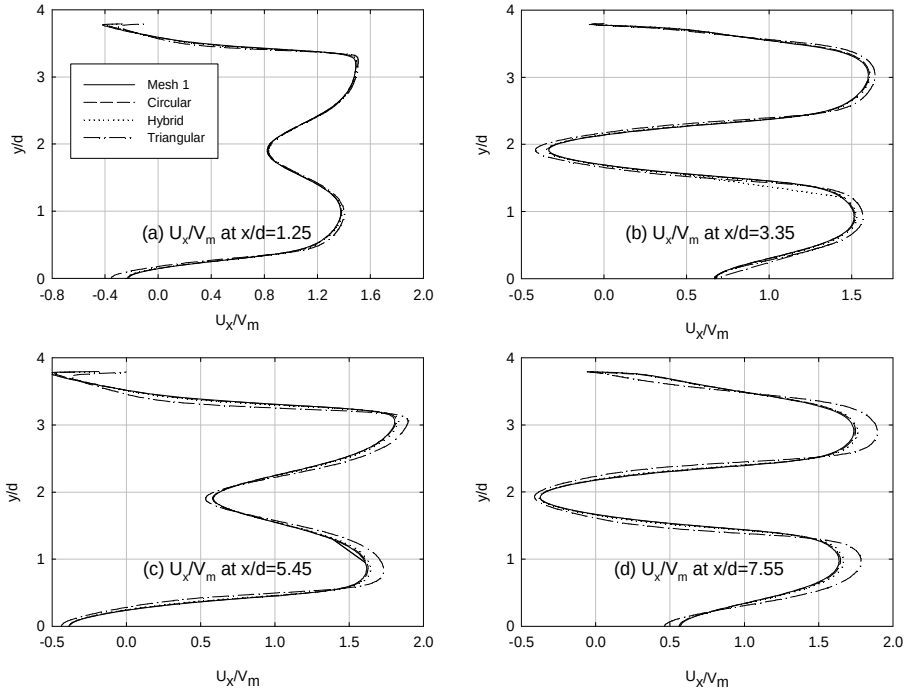

Figure 10. Simulated streamwise velocity profiles obtained with the κ-ω turbulence model (x/d = 1.25, 3.35, 5.45 and 7.55).

6. Study the effect of algorithms

The experimental conditions given in references [11-13] are used to study the effects that particular algorithms implemented in FLUENT may have on the simulations. To this aim both SIMPLE and Coupled schemes are applied and results of the simulations are numerically sampled at the locations shown in Figure 3.

Figures 11-13 show a comparison of velocity profiles obtained with the aforementioned algorithms by using both the κ-ε and the κ-ω models. Velocity fields are calculated using the enhanced mesh presented in Figure 2b. Only calculations performed with κ-ε and κ-ω models are presented, while similar simulations carried out with the κ-ε RNG model are not discussed. The results are, in all the cases, almost identical. Simulations performed using SIMPLE and Coupled algorithms lead to very close results. However, it is observed that the κ–ω model yields slower convergence when SIMPLE is used, while the κ-ε Realizable model is not able to converge when the same algorithm is invoked.

The comparison of predicted pressure differences at different locations in the channel are summarized in Table 4. Contrary to the comparison of velocity profiles, pressure losses are calculated using the circular mesh structure shown in Figure 6a. As shown in the table, the κ-ε and κ-ε RNG turbulence models predict almost the same pressure difference. This is not the case, however, for κ-ε Realizable and κ-ω models. It is noted that during this part of the work the κ-ε Realizable model was not able to smoothly converge. Nevertheless, it is observed that both SIMPLE and Coupled algorithms are equivalent when the κ-ε turbulence model is implemented. It is also observed that the Coupled algorithm always unconditionally converges; instead SIMPLE seems to be more cumbersome even if quite low under-relaxation coefficients are used. For instance, for in-line tube-bundles, the SIMPLE algorithm does not converge at all. Further, the Coupled algorithm produces very small residuals which enable a better precision to be achieved. In general, a single iteration is more expensive when the Coupled algorithm is used. In practice this means that for a domain requiring a large number of cells, the Coupled algorithm necessitates more computation time per iteration than SIMPLE. Nevertheless, it requires a lower number of calculation cycles. It is clear then, that a trade-off between these conditions must be established. Thus, for large number of meshes and for staggered tubes-bundles we recommend using SIMPLE with low under-relaxation coefficients in conjunction with κ-ε or κ-ε RNG turbulence models.

Table 4. Comparison of simulated pressure drop obtained with SIMPLE and Coupled algorithms.

	Δp_1 (Pa) SIMPLE	Δp_1 (Pa) Coupled	Difference (%)	Δp_2 (Pa) SIMPLE	Δp_2 (Pa) Coupled	Difference (%)
κ-ε	40.98	40.94	0.098	41.31	41.28	0.073
κ-ε Realizable	42.89	42.89	0	43.18	41.11	4.79
κ-ε RNG	39.97	39.99	0.05	39.23	39.21	0.05
κ-ω	100.37	102.43	2.05	43.10	46.26	7.33

* $\Delta p_1 = (P_{tap1} - P_{tap2})$; $\Delta p_2 = (P_{tap2} - P_{tap3})$

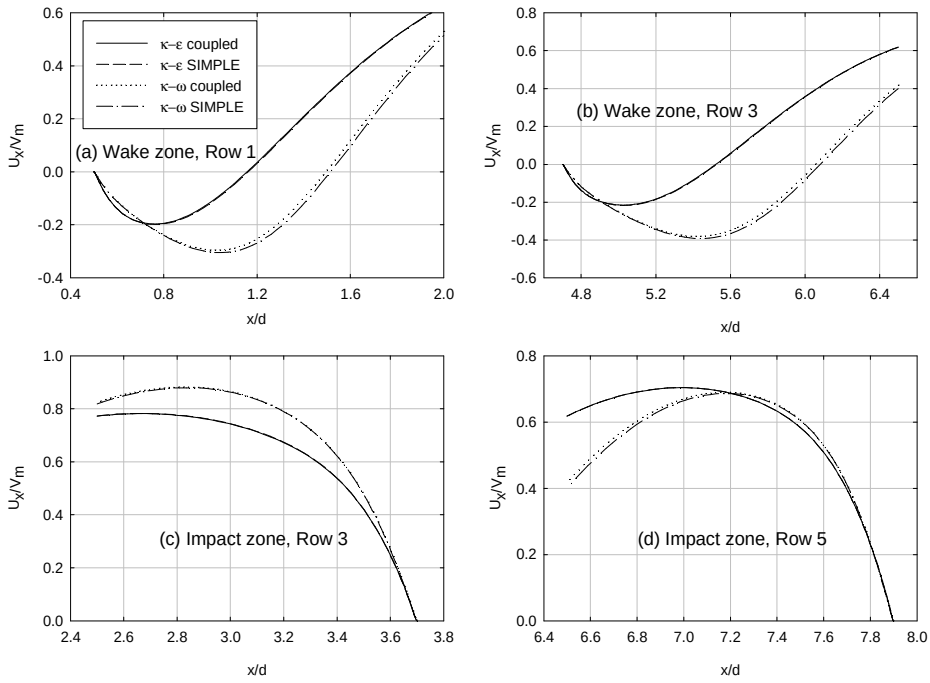

Figure 11. Comparison of streamwise velocity profiles obtained with SIMPLE and Coupled algorithms using κ-ε and κ-ω turbulence models (y/d=0).

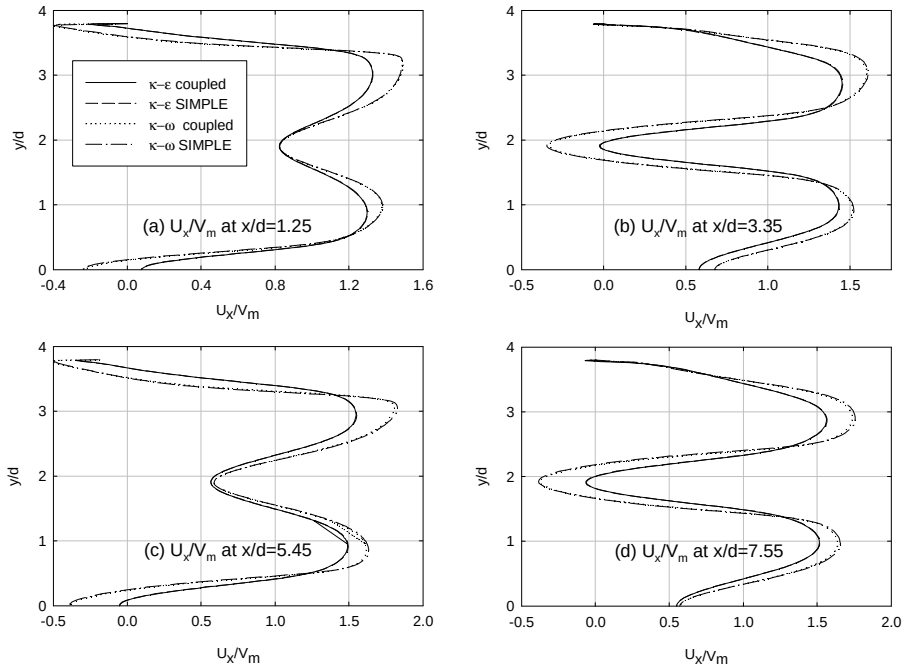

Figure 12. Streamwise velocity profiles obtained with SIMPLE and Coupled algorithms using κ-ε and the κ-ω turbulence models (x/d=1.25, 3.35, 5.45 and 7.55).

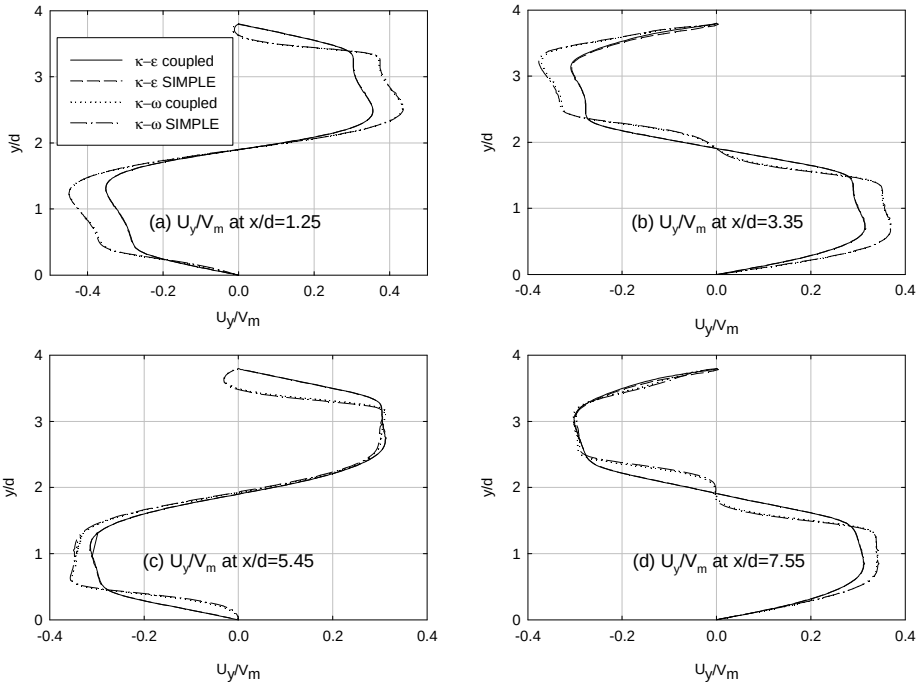

Figure 13. Transverse velocity profiles obtained with SIMPLE and Coupled algorithms using κ-ε and the κ-ω turbulence models (*x*/*d*=1.25, 3.35, 5.45 and 7.55).

7. Comparison of numerical simulations with data

Numerical simulations of flow velocity profiles as well as pressure drops are compared with experimental data collected by using in-line and staggered tube bundles, taken from [6, 11-13, 15]. Unfortunately, available information about pressure drop data is very scarce. Therefore, to reproduce the experiments, in some cases, correlations proposed by different authors are used to generate the "experimental" pressure drop conditions.

7.1 Comparison of calculated flow velocities with data

Figure 14 shows the comparisons of simulated average streamwise velocities as function of the normalized axial location with PIV data [13]. Different turbulence models are tested while the enhanced square-based mesh shown in Figure 2b is used to discretize the integration domain. Measurement uncertainties at 95% confidence level in mean velocity are ±3% in the central portion and ±5% close to the tubes.

It can be observed that all turbulence models produce correct trends. Nevertheless, it is apparent that the κ–ω model predicts quite well the velocity in the wake zone of row 1 (Figure 14a), but it is unable to follow the data in the wake region of row 3 (Figure 14b). Instead, in this flow location the κ–ε Realizable model seems to do a much better job. In this region, the κ–ω model over- predicts the experimental trends by up to 30% in the recirculation zone while other turbulence models are unable to produce acceptable results. In the impact zone of row 3, the predictions are close to the experimental

data, however, all turbulence models under-predict the velocities (Figure 14c). This behavior is much apparent within the impact region of row 5 (Figure 14d).

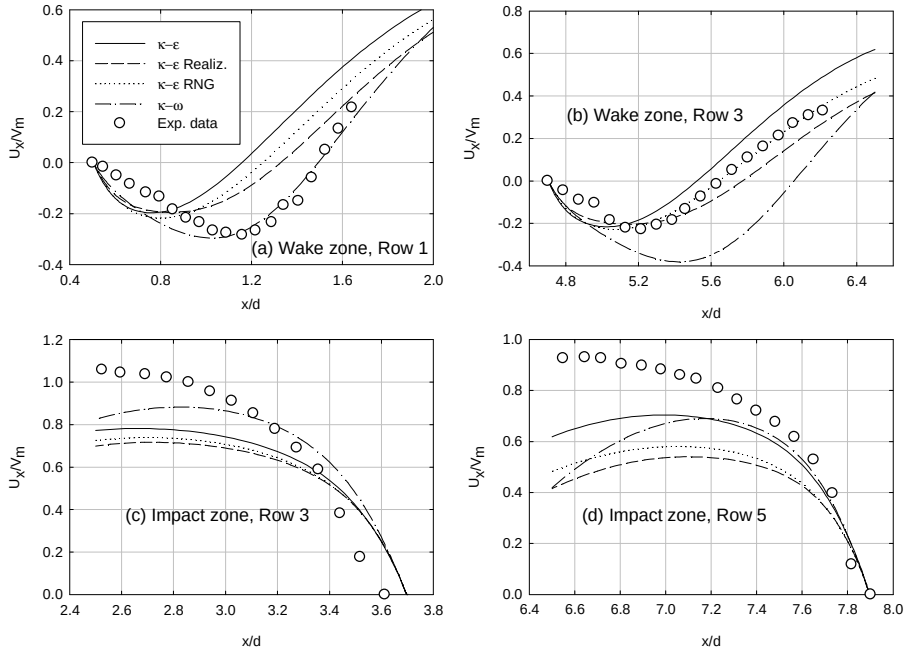

Figure 14. Comparison of simulated streamwise velocity profiles with data of Paul et al. [17] (axial location y/d=0).

We are concerned about possible systematic errors that could have been involuntary introduced during the experiments. In fact, the comparison of Figures 14a with 14c and Figures 14b with 14d, indicates that there is almost a perfect continuity along simulated values. Compare for instance the values of $U_x/V_m \approx 0.6$ at x/d=2 in Figure 14a with $U_x/V_m \approx 0.7$ at x/d=2.4 in Figure 14c where the values are not only close but they have the right extrapolation slope. The same observation can be drawn from Figures 14b and 14d. In turn, at the same location the experimental data are not only quite different but their extrapolation trends diverge. This argument seems to be supported by simulations of the lateral velocity profiles (Figures 15 and 16), which are quite good. In general, it is observed that all turbulence models are able to predict the lateral velocities for a wide range of axial locations. In the flow developing region (i.e., $0.85 < x/d < 3.35$), Paul et al. [13] argued that the ω-based model produces results that are in better agreement with the data, while in the spatially periodic region (i.e., $x/d > 5.05$) the ε -based ones are superior. It is obvious that from the streamwise velocities shown in Figure 14, it is impossible to validate this conclusion. However, all turbulence models are able to predict the experimental trends of transverse velocity profiles, but they are unable to reproduce the peaks that occur in the flow developing region. Since the κ-ω model is more sensitive to the mesh structure than κ-ε models, it requires more calculation time and it does not necessarily improve the simulation. Thus, to perform this kind of simulations, κ-ε based turbulence models are recommended.

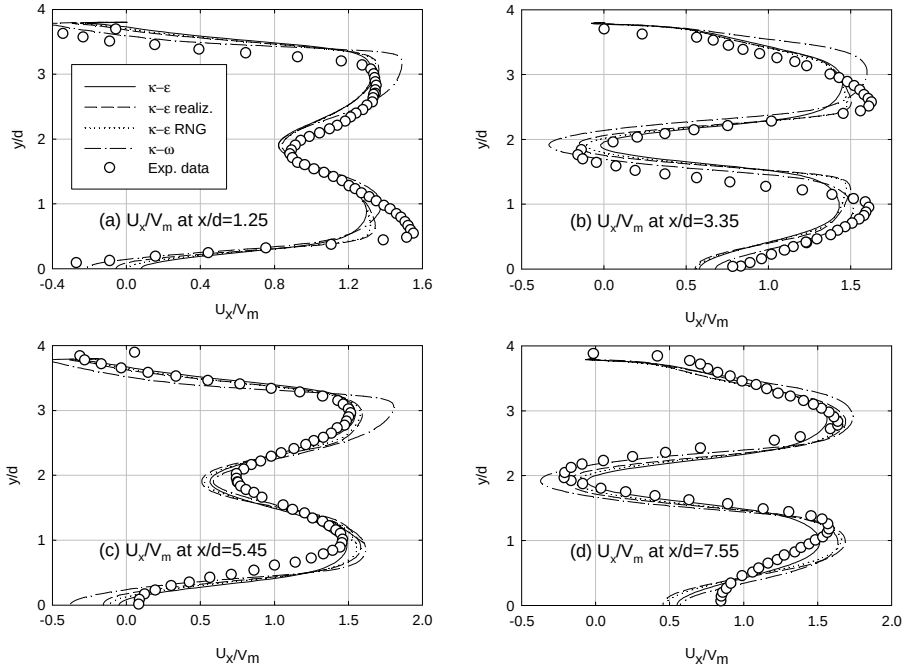

Figure 15. Comparison of simulated lateral velocity profiles with data [13] (x/*d*=1.25, 3.35, 5.45 and 7.55).

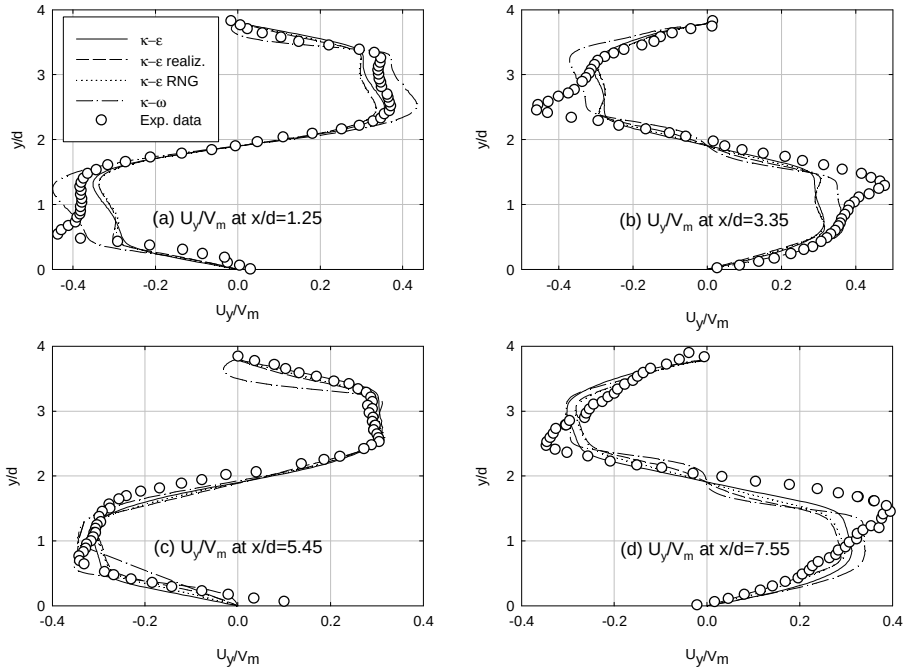

Figure 16. Comparison of simulated lateral velocity profiles with data [13] (*x*/*d* =1.25, 3.35, 5.45 and 7.55).

7.2 Comparison of calculated pressure differences with data

Pressure drops are simulated in both in-line and staggered tube-bundles and the results are compared with available data. With the exception of the work of Hadaller et al. [6] most of known works do not provide detailed pressure drop information. Instead, they present the data in terms of Pressure Loss Coefficients (PLCs). Unfortunately, none of these works provide enough details on how and where pressures are measured for determining coefficients and related correlations. For that reason, in this part of the work, numerical simulations are compared with data given in Hadaller et al. and Balabani & Yianneskis [15] by expressing the results in terms of PLCs. Regrettably, the accuracy of the correlations are not given in the literature. To this aim, pressure coefficients are calculated according to the correlation proposed by Balabani & Yianneskis, given as:

$$PLC = \frac{\Delta P}{N \rho \frac{V^2}{2}} \tag{6}$$

where N represent the row number and V an average velocity differently defined by different authors. It is obvious that the PLC calculated with Equation 6 represents an average value for each row. Thus, this equation does not explicitly take into account any possible dependency of flow pressure due to the location of the row inside the channel. Hadaller et al. and the Balabani & Yianneskis have proposed correlations for calculating the PLC in different tube-bundle configurations as a function of the Reynolds number. In general Hadaller et al., Balabani & Yianneski and Zukauskas [9] among others, have observed that in sub-critical incompressible flows, the pressure drop coefficient given by Equation 6 decreases with increasing the Reynolds number. Since data of Balabani & Yianneskis [15] are given in terms of the pressure drop coefficient per row, it makes quite difficult to compare them with numerical simulations. However, a particular effort is carried out to validate FLUENT calculations. To this aim, the correlations proposed by Balabani & Yianneskis are used; for in-line and staggered tube-bundles they are respectively given as:

$$PLC_{in-line} = .584 * \mathrm{Re}_{\max}^{-0.169} \tag{7}$$

$$PLC_{staggered} = .956 * \mathrm{Re}_{\max}^{-0.138} \tag{8}$$

Where the maximum Reynolds number Re_{max} is calculated using cylinder's diameter and the maximum average velocity u_{max} is determined over the smallest flow cross-sectional area of the channel. Thus, present simulations are performed using the following values: V_m= 0.93 *m/s*, u_{max}=1.291 and Re_{max}=12 858. For in-line and staggered tube-bundles average numerical values are determined along the locations shown in Figures 17a and 17b respectively.

We have observed that numerical results follow the expected behavior; thus, the static pressure starts increasing just in front of the cylinder and reaches a maximum in the stagnation region. In the downstream region, a pressure recovery is observed until the next cylinder region is reached where a similar trend repeats. To capture these features and to obtain appropriate pressure drop per row, virtual pressure taps are located between two consecutive rows as shown in Figure 17. Furthermore, to estimate the total pressure loss along the channels the pressure taps are placed far away from the first and last row of tubes. Hence, it is assumed that the major contribution to the total pressure drop is caused by the presence of the cylinders while the effects of friction over the walls of the channel are assumed to be small.

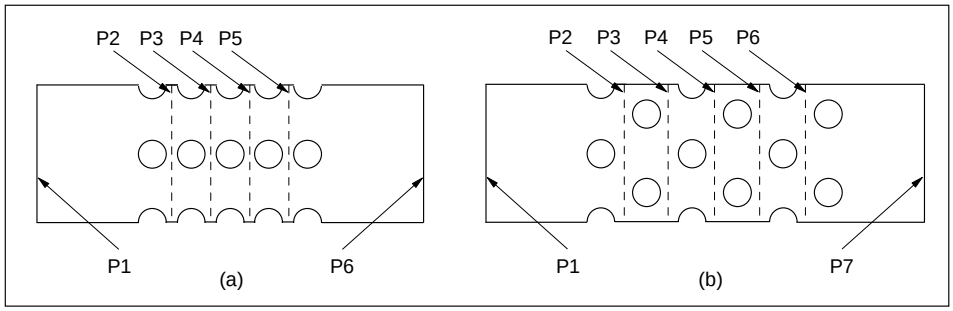

Figure 17. Schematics of: (a) in-line and (b) staggered tube-bundles with surfaces used for pressure drop calculations.

Estimated pressure differences obtained from simulations carried out using different turbulence models for in-line tube-bundles are summarized in Table 5. Because of the scarce information available on the experimental data, only relative errors for the calculated total pressure drop along the channel are given in the table. They are determined with respect to corresponding values estimated using the correlation (Equation 7), which is assumed to correctly represent the experimental trends.

Table 5. Comparison of pressure drop for in-line tube-bundles.

Pressure Difference (*Pa*)	κ-ε	κ-ε Realizable	κ-ε RNG	κ-ω
$(P_2\text{-}P_1)$	-44.73	-18.22	-31.76	117.25
$(P_3\text{-}P_2)$	-54.72	-50.25	-52.59	-60.27
$(P_4\text{-}P_3)$	-47.02	-41.16	-43.76	-25.41
$(P_4\text{-}P_2)$	-146.47	-109.63	-128.11	31.57
$(P_6\text{-}P_1)$	**-327.26**	**-294.35**	**-302.23**	**-308.03**
$\frac{(\Delta P_{6-1})_{corr} - (\Delta P_{6-1})_{simul}}{(\Delta P_{6-1})_{corr}}$	28%	35.3%	33.6%	32.3%

Pressure drop predictions are very sensitive to the location of the virtual taps. With the exception to pressure drops determined in the inlet and outlet flow regions, κ–ε based turbulence models produce similar results. In these regions the differences among predicted values are much higher, while the κ–ω model produces unphysical huge pressure gains. Note that the expected experimental value estimated with the correlation (7) is equal to 91 *Pa*/row. Zukauskas [9] observed that the experimental pressure drop per row decreases along the flow while the pressure gradient per row, after a given number of rows, remains almost constant. Unfortunately, this observation cannot be extended to the present simulations that show mostly random fluctuations. Nevertheless, simulated overall pressure differences along the channel are reasonably good. Due to the methodology used to estimate experimental values, we consider that errors of about 30% are acceptable. However, in general it can be observed that the simulations under-estimate the total pressure drop. The standard κ–ε model seems to be the more appropriate to treat pressure drop for in-line tube-bundle systems. Expected experimental pressure differences for a staggered tube-bundle are determined using correlation (8). For this type of bundle the pressure drop per row depends on the location of the pressure taps; thus, the pressure drop is equal to 215 *Pa*/row in the entrance region. Comparisons between estimated experimental data with results of the simulations are summarized in Table 6. Similar to the in-line tube-bundle case, predicted pressure

differences are higher in both the inlet and the outlet zones. In particular the κ–ω turbulence model produces much higher results than the others. Concerning the total pressure difference along the channel it is observed that with respect to correlation (8) the κ–ε and κ–ω models appear to be more accurate.

Table 6. Comparison of pressure drop for staggered-tube bundles.

Pressure Difference (*Pa*)	κ-ε	κ-ε Realizable	κ-ε RNG	κ-ω
(P_2-P_1)	-213.27	-188.41	-183.72	-409.23
(P_3-P_2)	-176.24	-164.22	-156.65	-329.41
(P_4-P_3)	-150.70	-175.97	-162.83	-247.78
(P_5-P_4)	-151.21	-147.78	-137.70	-268.10
(P_5-P_2)	-691.42	-676.38	-640.90	-1254.52
(P_7-P_1)	**-902.43**	**-763.07**	**-738.14**	**-1553.75**
$\frac{(\Delta P_{7-1})_{corr} - (\Delta P_{7-1})_{simul}}{(\Delta P_{7-1})_{corr}}$	30%	40.8%	42.79%	20.4%

The principal goal of this work consists of validating the FLUENT for simulating the flow of the moderator in CANDU-6 reactors. To this purpose, Hadaller et al. [6] collected data using in-line and staggered tube-bundle test sections that simulate some portions of a CANDU calandria vessel. In addition, for estimating the PLC, the same authors proposed the following correlation:

$$PLC = 4.54 * \mathrm{Re}^{-0.172} \tag{9}$$

where the Reynolds number is calculated using the average test section inlet flow velocity. The location of the pressure taps used in the staggered and in-line tube-bundles are shown in Figures 18 and 19 respectively.

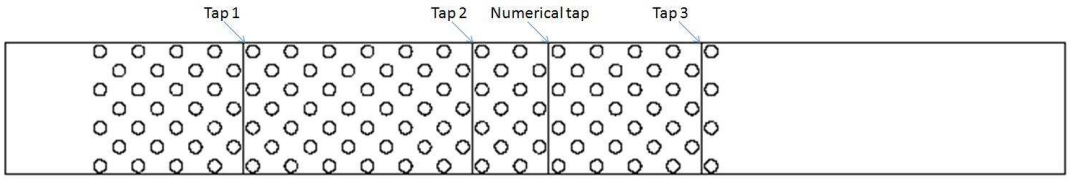

Figure 18. Schematic of the staggered tube-bundle test section and location of pressure taps, (Hadaller et al. [6]).

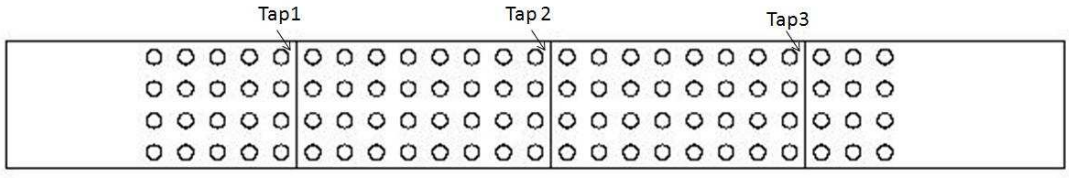

Figure 19. Schematic of the in-line test section and location of pressure taps, (Hadaller et al. [6]).

Comparisons between present pressure drop simulations with data, as well as results obtained with correlation (9) and predictions obtained with MODTURC code are given in Table 7.

Table 7. Pressure drop for in-line and staggered bundles

		V_m (*m/s*)	*T* (°*C*)	Re	Press. Loss Coeff.	Δ*p* (*Pa*) 16 rows		Δ*p* (*Pa*) 24 rows
						I*	S*	S
Stern Lab. T.P. 326	Experiments	0.054	39.5	2746	1.1630	28.2	N/A	N/A
	Correlation					26.92	26.92	40.38
	MODTURC					30.50	N/A	N/A
	κ-ε					**16.02**	**21.36**	**32.06**
	κ-ε R					**13.57**	**21.45**	**32.25**
	κ-ε RNG					**14.24**	**19.83**	**29.82**
	κ-ω					**7.28**	**29.67**	**44.11**
Stern Lab. T.P. 306	Experiments	0.070	63.6	5237	1.0408	41.30	N/A	N/A
	Correlation					41.66	41.66	62.50
	MODTURC					44.90	N/A	N/A
	κ-ε					**20.25**	**30.56**	**45.94**
	κ-ε R					**16.52**	**29.52**	**44.49**
	κ-ε RNG					**27.64**	**26.53**	**40.04**
	κ-ω					**12.21**	**46.65**	**69.47**
Stern Lab. T.P. 299	Experiments	0.103	79.8	9392	.9413	78.70	N/A	N/A
	Correlation					77.61	77.61	116.41
	MODTURC					87.30	N/A	N/A
	κ-ε					**36.38**	**61.96**	**93.21**
	κ-ε R					**27.55**	**55.33**	**84.69**
	κ-ε RNG					**30.69**	**48.45**	**73.47**
	κ-ω					**26.49**	**92.77**	**137.81**

* I = in-line and S = staggered; N/A = Not available.

It is clear that for any of the turbulence models, FLUENT is unable to correctly predict the experimental values. It is further observed that for the in-line tube-bundle, with exception of the pressure predicted with the κ-ε RNG model for the Test Point (T.P.) 306, the simulations strongly under-estimate the measurements (i.e., they are lower than half the experimental values). Instead, for the staggered tube-bundle, all turbulences models produce more reasonably predictions. In general, κ-ε models under-predict the data while the κ-ω model over-predicts the experimental trends. Nevertheless, this model provides the best values with a maximum relative error of about 18%. This error increases with increasing the Reynolds number. For the T.P. 326 and T.P. 299 the standard κ-ε model under-predicts the data by about 20% and for T.P. 306 by about 28 %. The κ-ε Realizable model behaves similarly to the standard κ-ε one, however, for high Reynolds the predictions get worse. In general, within a range of $\pm 30\%$, standard κ-ε and κ-ω models are able to predict the pressure drop in staggered bundles. This observation is in accordance to similar simulations given in [15]. However, any turbulence model is able to predict Hadaller et al. [6] in-line tube-bundle pressure drop data. It must be pointed out that in these experiments the pressure taps are fully located inside the bundle (see Figures 24 and 25); thus, it is quite possible that the flow in these regions is fully developed. Therefore, the κ-ω turbulence model seems to be able to better predict the pressure when the flow is fairly well developed.

The comparison of FLUENT with MODTURC simulations shows that the results of this code, at least for in-line bundles, are superior. This is quite obvious because this code uses the same experimentally determined hydraulic resistance terms to fit the data. In turn, FLUENT handles the complete set of Navier-Stokes equations without requiring empirical adjustments. Even though MODTURC pressure drop calculations for staggered-bundles are mentioned in Hadaller et al. [6], they do not provide prediction outcomes. Thus, it is not possible to compare results obtained with these two codes. However, for this particular case, FLUENT simulations are in good agreement with the experiments.

8. Conclusions

A series of numerical simulations of cross-flows in both in-line and staggered tube-bundles are performed using FLUENT-6 code. Several turbulence models in conjunction with different mesh-discretization structures are used to perform the calculations. The enhanced square mesh is simple, it does not require large number of cells to be used, and provides similar results obtained by using other meshes. Therefore, this type of mesh is strongly recommended. The results show that the κ-ω turbulence model is quite sensitive to both the mesh type and mesh refinement. In turn, beyond a certain refinement, κ-ε based models seem to be almost independent of these parameters. In addition different algorithms available in FLUENT are also tested. It is shown that the Coupled pressure-based algorithm is able to handle both staggered and in-line tube-bundle systems, producing properly convergence results for all turbulence models. In turn, the SIMPLE algorithm is not able to 'simply' converge for in-line tube-bundles. Using low under relaxation coefficients allows, however, this algorithm to converge, but at a much slower pace than the coupled and to a lesser accuracy. Nevertheless, when a large number of cells are used, SIMPLE in conjunction with κ-ε and κ-ε RNG model considerably reduces the computational time. When this criterion is not a constraint and a higher accuracy is required, the use of the Coupled algorithm is strongly recommended. All turbulence models available in FLUENT are able to predict experimental flow velocity profiles taken from references [11-13]. Instead, κ-based two equation models fail to predict velocity and pressure in in-line tube-bundles; however, they produce reasonable good results for staggered tube-bundles. This particular behavior is possible due to the fact that flow mixing is more important in staggered-bundles; thus, the flow achieves its development much faster than in in-line tube-bundles. In general κ-ε based models tend to under-predict the pressure drop while the κ-ω model over-predicts the experimental trends. The κ-ε models are able to predict the pressure drop in the tube bundles, whereas the κ-ω model seems to predict well developed flows but has some difficulties for catching the data in both the first and last row regions of tubes. Even though the numerical results obtained for Hadaller et al. [6] staggered tube bundle experiments are relatively good; it should be interesting to validate the simulations with velocity profile data. Even though, according to the authors' knowledge, such information is very scarce or does not exit. The use of standard κ-ε and κ- ω models are recommended to perform these types of simulations. Numerical results obtained during the present work should help us to implement full moderator flow simulations in CANDU nuclear power reactors using FLUENT code.

Acknowledgments

This work is funded by the NSERC Discovery Grant RGPIN 41929 and the Hydro-Québec chair in nuclear engineering.

References

[1] Huget R.G., J. Szymanski & W. Midvidy, 10th Annual Conf. CNS Ottawa, Canada, 1989.

[2] Huget R.G., Szymanski J., Galpin P.F. & W. Midvidy, 3th Int. Conf. Simul. Methods Nucl. Eng., Montréal, 1990.

[3] Yoon C., Rhee B.W. & B.J. Min, Nucl. Tech., vol. 148, pp. 259-267, Dec 2004.

[4] Yoon C., Rhee B.W., Kim H.T., Park J.H. & B.J. Min, J. Nucl. Sci. Tech., vol. 43, pp. 505-513, 2006.

[5] Yoon C. & J.H. Park, Annals of Nuclear Energy, vol. 35, pp. 1041-1049, 2008.

[6] Hadaller G.I., Fortman R.A., Szymanski J., Midvidy W.I. & D.J. Train, 17th CNS Conf., Fredericton, New Brunswick, Canada, 1996.

[7] Kim M., Yu S.-O. & H.-J. Kim, Nucl. Eng. Design, vol. 236, pp. 1155-1164, 2006.

[8] Bouquillon M., « Modélisation numérique de jets et leurs applications dans la simulation des écoulements dans la cuve du réacteur CANDU » Maîtrise es sciences appliquées, École Polytechnique de Montréal, 2008.

[9] Zukauskas A., "High-Performance Single-Phase Heat Exchangers," Hemisphere Publishing Co., New York, USA., 1989.

[10] Beale S.B. & D. B. Spalding, Journal of Fluid and Structures vol. 13, pp. 723 - 754, 1999.

[11] Paul S.S., "Experimental and Numerical Studies of Turbulent Cross-flow in a Staggered Tube Bundle," Mechanical Engineering, Winnipeg, Manitoba, Canada, University of Manitoba, 2006.

[12] Paul S.S., Tachie M.F. & S.J. Ormiston, Int. J. Heat and Fluid Flow, vol. 28, pp. 441-453, 2007.

[13] Paul S.S, Ormiston S.J. & M.F. Tachie, Int. J. Heat and Fluid Flow, vol. 29, pp. 387-414, 2008.

[14] Liang C. & G. Papadakis, J. Fluid and Structures, vol. 23, pp. 1215 - 1230, 2007.

[15] Balabani S. & M. Yianneskis, Proc. Institution Mech. Eng.: Part C J. Mech. Eng. Sci., vol. 210, p. 317, 1996.

[16] Simonin O. & M. Barcouda, Proc. 4th Int. Symp. App. of Laser Anemometry to Fluid Mechanics, Lisbon, Portugal, 1988.

[17] Launder B.E. & D.B. Spalding, "Lectures in Mathematical Models of Turbulence," London, England, Academic Press, 1972.

[18] Shih T.H., Liou W.W., Shabbir A., Yang Z. & J. Zhu, Comp. Fluids, vol. 24, pp. 227 - 238, 1995.

[19] Yakhot V. & S.A. Orszag, J. Sci. Comp., vol. 1, pp. 1-51, 1986.

[20] Wilcox D.C., "Turbulence Modeling for CFD," California, DCW Industries, INC, 1998.

[21] Menter F.R., AIAA Journal, vol. 32, pp. 1598 - 1605, 1994.

[22] FLUENT User Guide, 2005.

[23] Patankar S.V., "Numerical Heat Transfer and Fluid Flow," New York, Hemisphere Publishing Corporation, 1980.